LHC discovery potential of the lightest NMSSM Higgs in $h \to a_a \to \mu\mu\mu\mu$ channel

Alexander Belyaev,[1,2] Jim Pivarski,[3] Alexei Safonov,[3] and Sergey Senkin[3]

[1] *School of Physics & Astronomy, University of Southampton, Highfield, Southampton SO17 1BJ, UK*

[2] *Particle Physics Department, Rutherford Appleton Laboratory, Chilton, Didcot, Oxon OX11 0QX, UK*

[3] *Physics Department, Texas A&M University*

(Dated: August 23, 2009)

We explore the potential of Large Hadron Collider to observe $h_1 \to a_1 a_1 \to 4\mu$ signal from the lightest lightest scalar Higgs boson (h_1) decaying into two lightest pseudoscalar Higgs bosons(a_1) followed by their decays into 4 muons within the Next-to-Minimal Supersymmetric Standard Model (NMSSM). The signature under study allows to cover the NMSSM parameter space with M_{a_1} below 3.5 GeV and large $Br(h_1 \to a_1 a_1)$ which has not been studied previously. In case of such a scenario, the suggested strategy of the observation of 4μ signal with the respective background suppression would provide a unique way to discover the lightest scalar NMSSM Higgs boson.

PACS numbers: 13.38.Dg 13.38.Qk

Contents

I. INTRODUCTION

The next-to-minimal supersymmetric standard model (NMSSM) [1–13] is extended by one singlet superfield in addition to the particle content of the Minimal Supersymmetric Standard Model (MSSM) and due to this design has several new attractive features as compared to MSSM. First of all, NMSSM elegantly solves so called μ-problem [14]: the scale of the μ-parameter is automatically generated at the electroweak or SUSY scale when the singlet Higgs acquires a vacuum expectation value. On the other hand NMSSM can solve fine-tuning and little hierarchy problems of MSSM [15]. The upper mass limit on the lightest CP-even Higgs boson in NMSSM is larger than in MSSM and since more parameter space survives LEP II bounds from the Higgs search, NMSSM is less fine-tuned. On the other hand there is additional mechanism for the reduction of fine-tuning since LEP II bounds from the Higgs search can be partly avoided if the branching of $h_1 \rightarrow a_1 a_1$ decay is significant (h_1 and a_1 stands for the lightest CP-even and CP-odd Higgs bosons respectively). This decay channel of h_1 diminishes the branching ratios for conventional modes used in direct Higgs searches and largely softens direct Higgs boson mass limits from LEP.

One should stress that due to the extended scalar sector (in comparison to MSSM) NMSSM offers richer Higgs collider phenomenology [16–24] as well as richer cosmological Dark Matter implications related to the presence of the fifth neutralino ("singlino"), relic density for which can be achieved to be correct one [25].

The collider phenomenology of the Higgs sector of the NMSSM is very interesting in several aspects, therefore a short historical introduction is in order. In [17] the first attempt to establish 'no-lose' theorem for NMSSM has been done. This theorem states that LHC has a potential to discover at least one NMSSM Higgs boson in the conventional mode given that Higgs-to-Higgs decay modes are not important. However the point is that Higgs-to-Higgs decay modes can be important as has been shown and studied later on in analysis devoted to re-establishing of 'no-lose' theorem [18–24] for the case when $h_1 \rightarrow a_1 a_1$ decay is significant and a_1 is light. So far, the case of the lightest a_1 was explored for m_{a_1} below $2b$-quark threshold but above 2τ one, $2m_\tau < m_{a_1} < 2m_b$, establishing the scope of the 4τ channel in Higgs-strahlung and Vector Boson Fusion for the NMSSM No-Lose Theorem at the LHC [24]. Theses analysis require a substantial integrated luminosity (10-100 fb^{-1}) and quite challenging analysis in the technical sense.

In this paper we explore the mass region of a_1 with the mass below 2μ threshold: $m_{a_1} < 2m_\mu$. In this case, which has not been studied previously, we explore $h_1 \to a_1 a_1 \to \mu\mu\mu\mu$ signature. Unlike searches for 4τ signature, the measurement of invariant mass of muon pair provides a direct estimate of m_{a_1} which defines a clear set of the kinematical cuts for the background suppression. Further, this channel is essentially free of backgrounds and therefore allows to use direct gluon fusion production combined with $b\bar{b}$ fusion production instead of subdominant vector boson fusion or associate Higgs production processes used in case of 4τ signature to to suppress large QCD backgrounds.

We demonstrate that the analysis in the four muon mode has excellent sensitivity for Lightest CP-even NMSSM Higgs boson and can be performed with just a handful of first CMS data and requires very little in terms of detector performance except reasonably robust tracking for muons and well functioning muon system. To make this a realistic analysis, we use parameters of the CMS experiment in designing selections and estimating background contributions.

The rest of the paper is organized as follows. In Section II we study the NMSSM parameters space for which $m_{a_1} < 2m_\mu$ case of our study is realized. In Section III we perform signal versus background analysis and present our final results in Section IV. In Section V we draw our conclusions.

II. NMSSM PARAMETER SPACE AND SIGNAL PRODUCTION RATES

A. The model and the parameter space for the light a_1 scenario

In our study we consider the simplest version of NMSSM [1–12], where $\mu\widehat{H_1}\widehat{H_2}$ term of the MSSM superpotential is replaced by

$$\lambda\widehat{S}\widehat{H}_1\widehat{H}_2 + \frac{\kappa}{3}\widehat{S}^3 \tag{1}$$

which makes superpotential scale invariant. In addition, we have five soft braking terms in general, "non-universal" case:

$$m^2_{H_1}H_1^2 + m^2_{H_2}H_2^2 + m^2_S S^2 + \lambda A_\lambda H_1 H_2 S + \frac{\kappa}{3}A_\kappa S^3. \tag{2}$$

In the above equations the tilded capital letters denote superfield while non-tilded ones stand for the scalar component of the respective superfield.

Soft breaking parameters $m^2_{H_1}$, $m^2_{H_2}$ and m^2_S from Eq. 2 can be traded for M_Z, the ratio of the doublet Higgs vacuum expectation values (VEVs) $\tan\beta$, and $\mu = \lambda\langle S\rangle$ (where $\langle S\rangle$ denotes the VEV of the singlet Higgs field) through the three minimization equations of the Higgs potential. Therefore, assuming that the Higgs sector is CP conserving, the NMSSM Higgs sector at the Electro-Weak (EW) scale is uniquely defined by fourteen parameters: $\tan\beta$, the trilinear couplings in the superpotential λ and κ, the corresponding soft SUSY breaking parameters A_λ and A_κ, the effective μ parameter $\mu = \lambda\langle S\rangle$, the gaugino mass parameters M_1, M_2 and M_3, the squark and slepton trilinear couplings A_t, A_b and A_τ, and the squark and slepton mass parameters M_{f_L} and M_{f_R}. For simplicity, we assume here the universality within 3 generations for the last two parameters.

In the following we study the NMSSM parameter space, defined in terms of the above inputs, that survive present theoretical and experimental constraints. We make use of NMSSMTools package [26–28] to scan the NMSSM parameter space and to identify the region of our interest, where $B_{h\to aa}$ is dominant over the MSSM (conventional) Higgs boson decay modes $B_{h\to WW^*,\, b\bar{b},\, \tau^+\tau^-}$.

We have performed two scans "wide" and "narrow," where the narrow scan focuses more exclusively on the region with dominant $B_{h\to aa}$.

I do not observe a big difference between two scans which would make them called "wide" and "narrow". I believe that wide scan is too narrow, especially for A_κ which is general in the hundreds of GeV range. Scans are uniform in each parameter listed in Table I, subject to phenomenological and experimental constraints except for the specialized LEP $h\to aa$ searches. The λ and A_κ parameters are restricted even in the wide scan to yield small m_a values, important for large $B_{a\to\mu\mu}$. In particular, we have restricted A_κ to be in the really narrow range motivated by the recent study [24]. Furthermore, in our study we have found that important parameter for distinguishing between conventional Higgs decays and $h\to aa$ decays is the ratio of κ over λ, so we perform uniform scans in this ratio, rather than κ alone.

Our first results of wide scan are presented in Fig 1 which demonstrates quite know fact that in allowed NMSSM parameter space two most probable scenarios the lightest CP-even Higgs boson take place. In the first scenario the scalar Higgs is the SM-like, obeys SM/MSSM LEP constraints [29, 30] to be above about 115 GeV and decays primarily into conventional WW^*, $b\bar{b}$, and $\tau^+\tau^-$ modes as one can see from see Fig. 1(right).

TABLE I: Ranges for NMSSM parameter scans. The narrow scan focuses on the region with large $B_{h\to aa}$.

Wide scan	Narrow scan
$0 < \kappa/\lambda < 0.8$	$0 < \kappa/\lambda < 0.5$
$0 < \lambda < 0.1$	*same*
$-0.1 < A_\kappa < 0$ GeV	*same*
$0 < A_\lambda < 4$ TeV	$1 < A_\lambda < 3$ TeV
$100 < \mu < 200$ GeV	$100 < \mu < 150$ GeV
$10 < \tan\beta < 60$	$10 < \tan\beta < 33$

The other scenario occurs when the lightest CP-even Higgs boson has dominant singlet component, i.e. it is almost a singlet. In this case, such a Higgs boson can be very light surviving LEP constraints [29, 30] and dominantly decays into the pair of CP-odd Higgs bosons $h_1 \to a_1 a_1$ which are also have dominant singlet component. Being an almost singlet in this scenario, lightest CP-even Higgs boson interacts weakly with SM fermions and gauge bosons and this allows it to escape LEP constrains even if its mass as low as 20 GeV.

Jim, could you please check if h_1 as light as 20 GeV survives from the scan? Fig.1(left) shows that there are no 20 GeV h_1 survived. I am not sure it is correct. Could you check, please as well as check the Fig.1 caption?

Fig 2 demonstrates the clear correlation between m_{a_1} and λ(left) as well as m_{a_1} and A_{kappa}(right) in terms of density of randomly scattered points (**would also good to have plots for m_{a_1} vs κ/λ since κ/λ is our principle parameter**). We can see that if the mass of a_1 is below its τ threshold decay then λ is confined to be below 0.1 while A_κ is confined to be $|A_\kappa| < 0.1$ (**Jim, please, check this statement from the wider scan**).

It is also essential to stress that $m_{a_1} < 2m_\tau$ condition forces the lightest CP-odd Higgs a_1 to be the singlet with very good accuracy. It's non-singlet admixture is below 1%, while for the lightest CP-even Higgs boson, h_1 two scenarios can be realized as mentioned above. In Fig. 3 we present the distribution of the admixture of the singlet component of the h_1 in the $m_{a_1} - m_{h_1}$ plane.

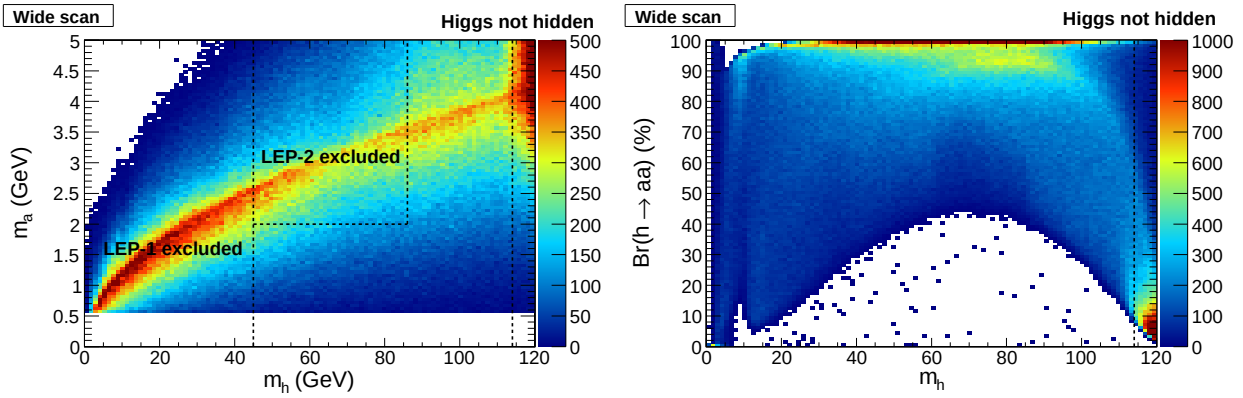

FIG. 1: Left: regions of m_a vs. m_h excluded by LEP searches, right: the strong correlation between m_h and $B_{h\to aa}$. The above scan is subject to experimental constraints (other than the two specialized LEP searches for $h\to aa$) which require a conventionally-decaying Higgs to have $m_h > 114$ GeV.

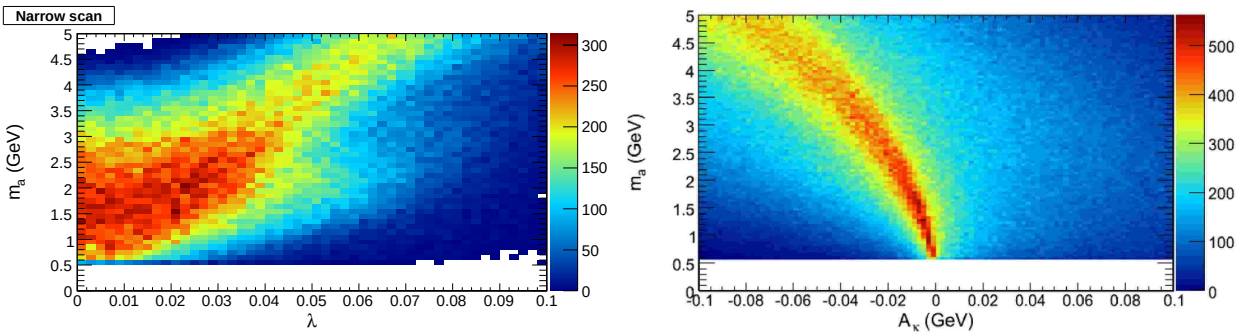

FIG. 2: Both λ and A_κ must be close to zero for m_a to be below the $2\,m_\tau$ threshold.

One see that singlet component is dominated over the whole parameter space subject of our scan except the region of the m_{h_1} around 120 GeV when h_1 is essentially SM-like. When the h_1 is essentially singlet, then role of the SM-like Higgs is played by the next-to-lightest CP-even Higgs boson, h_2. In Fig. 4 we illustrate this presenting singlet and non-singlet admixture of h_1 in $m_{h_2} - m_{h_1}$ plane.

B. The h_1 and a_1 branching ratios

Since a_1 is essentially singlet, the singlet admixture of h_1 defines its coupling to a_1 and the respective branching ratio $Br(h_1\to a1a_1)$ as illustrated in Fig. 5 which presents singlet

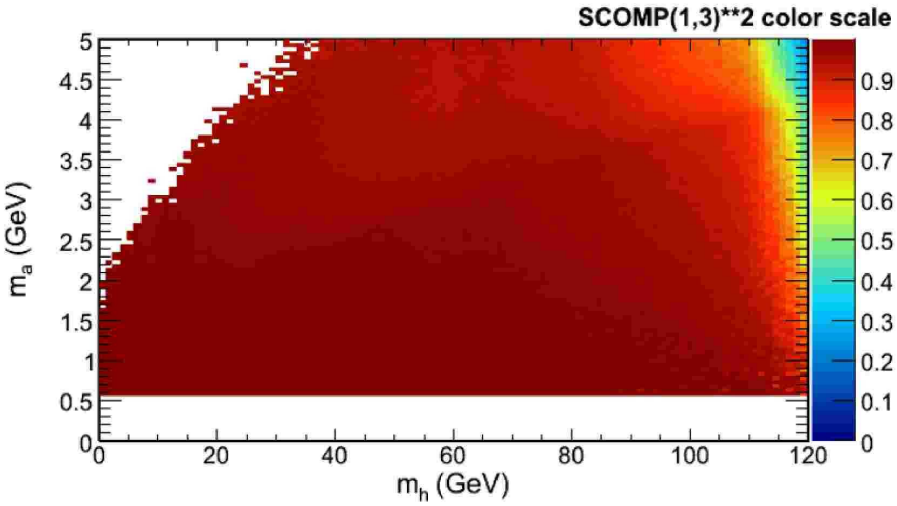

FIG. 3: Distribution of the admixture of the singlet component of the h_1 in the $m_{a_1} - m_{h_1}$ plane

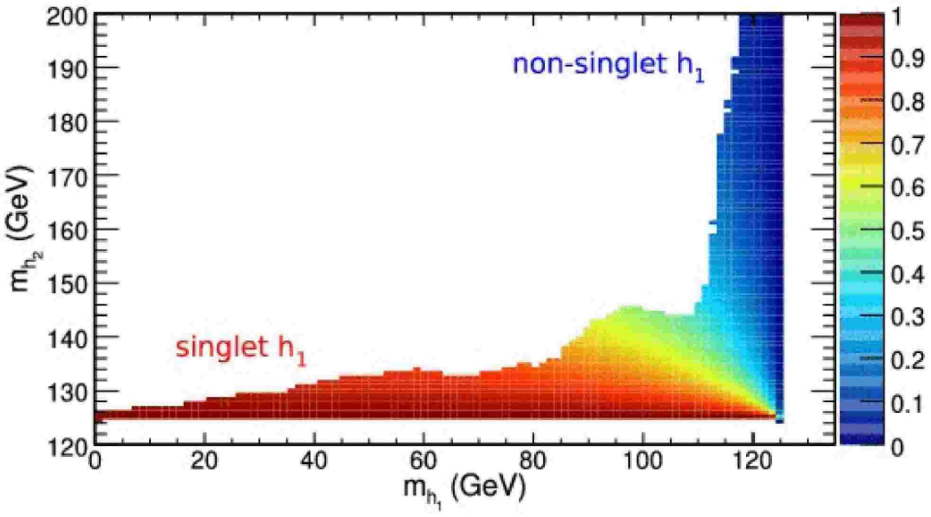

FIG. 4: Singlet and non-singlet admixture of h_1 in $m_{h_2} - m_{h_1}$ plane

component of h_1 (mixing angle squared of the h_1 and the pure singlet state, which is given by `SCOMP(1,3)`^{2} parameter in NMSSM tools) versus $Br(h_1 \to a1a_1)$.

The essential parameter which controls the h_1 to be a singlet or non-singlet we have found to be the ratio of κ/λ (**I think we need a plot scomp(1,3)^2 vs κ/λ illustrating this**) which is eventually controls $Br(h_1 \to a1a_1)$ as demonstrated by $Br(h_1 \to a1a_1)$ vs κ/λ distribution in Fig. 6. One clearly see that for $\kappa/\lambda < 0.3$, the $Br(h_1 \to a1a_1)$ is significant which is related to the fact that the singlet component of h_1 is large. One can see that the

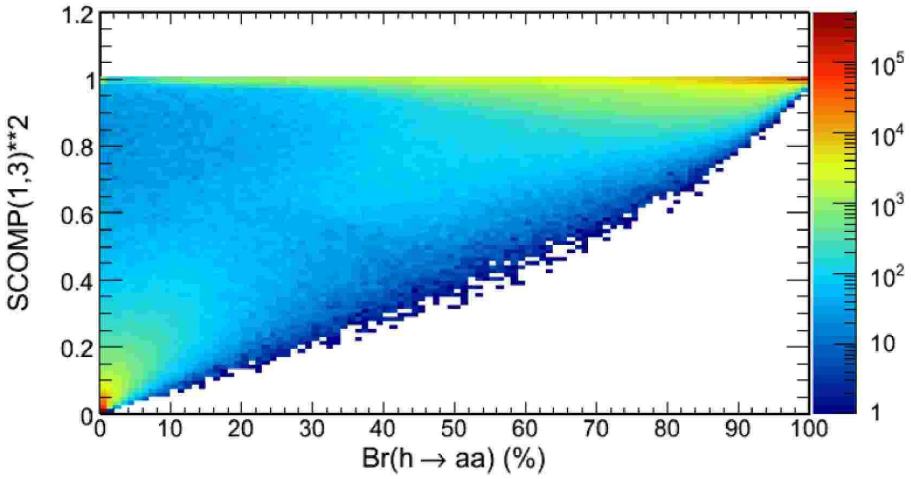

FIG. 5: Singlet component of h_1 (mixing angle squared of the h_1 and the pure singlet state) versus $Br(h_1 \to a1a_1)$

typical value of $Br(h_1 \to a1a_1)$ in this region is 70-100%. (**What are competing Br of h_1 in this region?**)

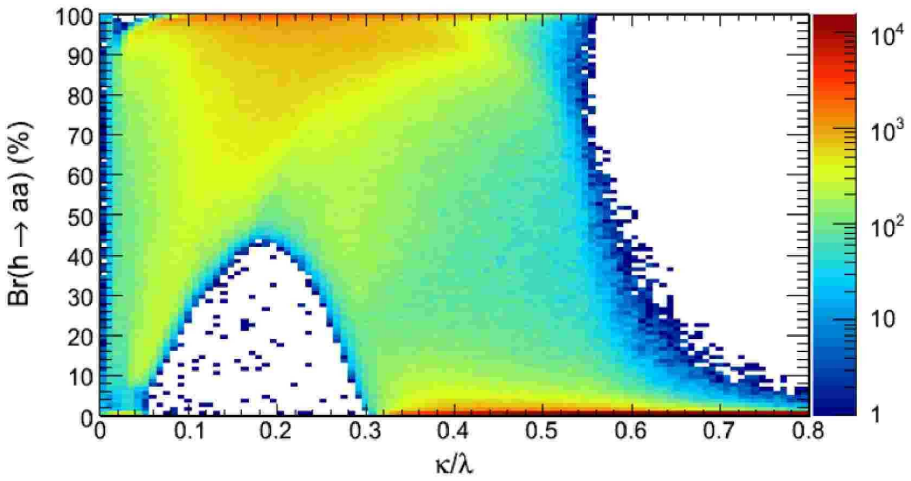

FIG. 6: $Br(h_1 \to a1a_1)$ vs κ/λ distribution.

The singlet and non-singlet features of the lightest CP-even Higgs boson, h_1, can be clearly disentangled in $\mu - \kappa/\lambda$ plane as one can see from Fig.7. For $mu \simeq 110$ GeV, h_1 becomes a singlet already for $\kappa/\lambda < 0.5$ while for $mu \simeq 200$ GeV h_1 turns to be a singlet when $\kappa/\lambda < 0.3$. One can clearly see that μ and κ/λ are essential variables defining the

property of h_1 of being singlet or non-singlet. (**Why μ parameter was chosen in this narrow 100-200 GeV range in our scan?**
One more remark/request: since μ and κ/λ are very important parameters for the h_1, I would like to ask you to make plot for the color map of $Br(h\to a_1a_1)$ in the same, (μ-κ/λ) plane – this would be Fig.7b.) Another representative plot separating

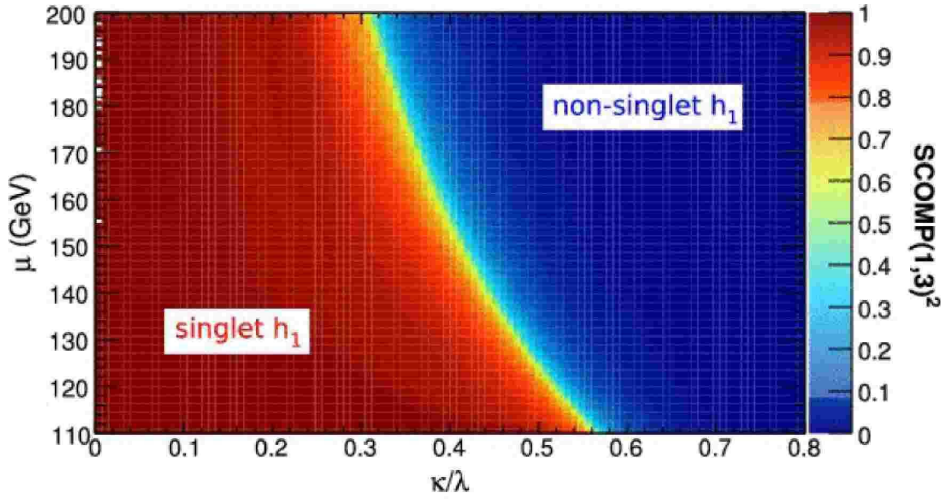

FIG. 7: The singlet and non-singlet features of the lightest CP-even Higgs boson, h_1, in $\mu - \kappa/\lambda$ plane.

singlet and non-singlet h_1 states is the scatter plot of the partial decay width $\Gamma(h_1\to a_1a_1)$ versus $\Gamma(h_1\to jj + bb + WW)$ shown in Fig.8. The red and blue dots here denotes h_1 being 90% singlet or 90% non-singlet respectively. (**Did you include $h_1\to\tau\tau$?**) One can see again how well singlet/non-singlet states are separated in the plane of these variables.

As we have mentioned above, $a1$ Higgs boson has extremely small non-singlet admixture in the region of our interest ($m_{a1} < 2m_\tau$), however even though its non-singlet component is very smaill, its branching ratio to $\mu^+\mu^-$ is large as soon as it kinematically allowed. In Fig.9 (left) we present how large the singlet component of the light a_1 can be versus $Br(a_1\to\mu\mu)$. In the Fig.9 (right) we show m_{a1} distribution in $\lambda - A_\kappa$ plain together with contour of the maximum value of $Br(a1\to\mu\mu)$ which is reached by at $m_{a1} \simeq 2$ GeV. (**I wanted to ask Jim the question about the meaning of the color. This point should be clearly explained from the very beginning, when we start presenting plots like these. The question is the following: for each point(small area) in $\lambda - A_\kappa$ plain we can have different values of m_{a1}. So, for the plot do you chose the max or min value**

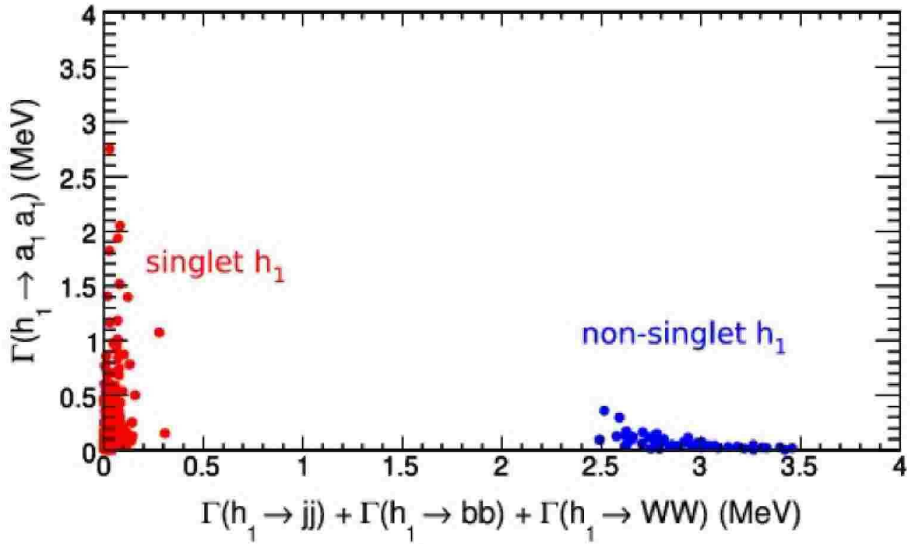

FIG. 8: Scatter plot of the partial decay width $\Gamma(h_1 \to a_1 a_1)$ versus $\Gamma(h_1 \to jj + bb + WW)$. The red and blue dots here denotes here that h_1 is being 90% singlet or 90% non-singlet respectively.

of the m_{a1} for the color map?
Another remark: eventually the left figure should be replotted in more sensible way)

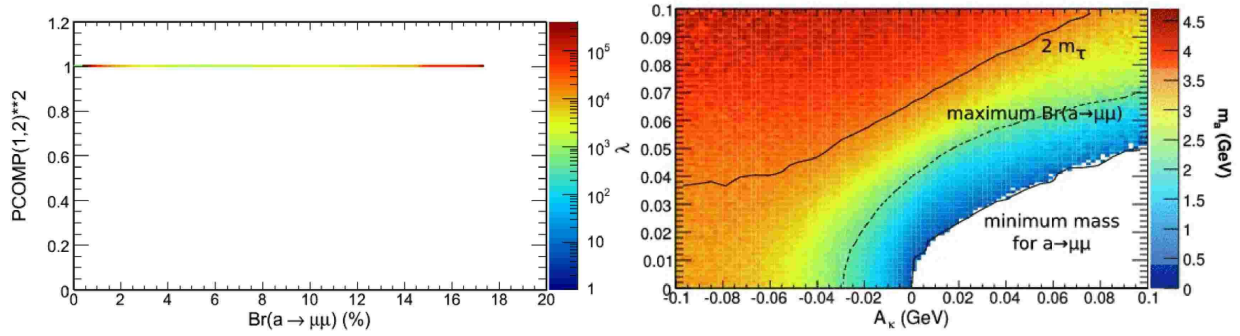

FIG. 9: Left: the value of singlet component of the light a_1 is versus $Br(a_1 \to \mu\mu)$. Right: m_{a1} distribution in $\lambda - A_\kappa$ plain together with contour of the maximum value of $Br(a1 \to \mu\mu)$ (dashed contour) which depends only on the kinematics defined by the m_{a1}.

In Fig. 10 we present the value of $Br(a_1 \to \mu\mu)$ versus m_{a1} which we have tabulated and use in our analysis. It is important to stress that for a given m_{a1} the value of $Br(a_1 \to \mu\mu)$ is essentially fixed and is practically independent off other model parameters. (**We need**

more details on how this Br is independent off other parameters and how large deviations from the red curve can be. We should probably have one more additional figure on this). We can see that $Br(a_1 \to \mu\mu)$ can be as large as 18% for

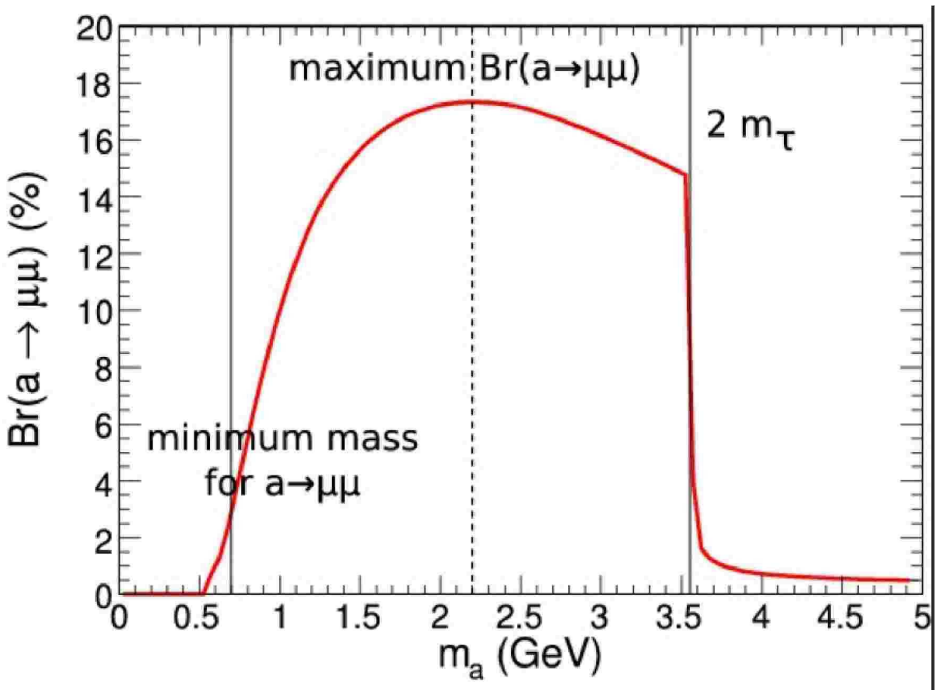

FIG. 10: The value of maximal $Br(a_1 \to \mu\mu)$ versus m_{a1}

m_{a1} around 2 GeV. In the mass range of interest (below the $a \to \tau^+\tau^-$ threshold), the main competing channels are $a \to gg$ and $a \to s\bar{s}$.

C. Production rates

As we have shown, the lightest CP-even Higgs boson, h_1, typically has significant singlet component in the region of our interest (i.e. in the region of $m_{a1} < 2m_\tau$) and as we have found above, both, $Br(h_1 \to a_1 a_1)$ and $Br(a_1 \to \mu\mu)$, are quite significant. In the same time, one should expect the suppression of the h_1 production rate since h_1 interacts weakly with the fermions and gauge bosons due to its singlet nature.

In our study we have evaluated $pp \to h_1$ production cross section for the $gg \to h_1$ and $b\bar{b} \to h_1$ process at the next-to-leading order (NLO) using the following procedure.

First, we have used HIGLU v2.102 package [31] to calculate SM Higgs production cross section in $gg \to H_{SM}$ process. Since the ratio of $\sigma(gg \to h_1)/\sigma(gg \to H_{SM})$ production cross

sections is equal to the ratio of partial decay widths $\Gamma(h_1 \to gg)/\Gamma(H_{SM} \to gg)$, one finds

$$\sigma(gg \to h_1) = \sigma(gg \to H_{SM}) \frac{\Gamma(h_1 \to gg)}{\Gamma(H_{SM} \to gg)} = \sigma(gg \to H_{SM}) \frac{Br(h_1 \to gg)\Gamma^{tot}(h_1)}{\Gamma(H_{SM} \to gg)}. \quad (3)$$

Therefore we have all components to evaluate $\sigma(gg \to h_1)$: we use $\sigma(gg \to H_{SM})$ and $\Gamma(H_{SM} \to gg)$ calculated using HIGLU at NLO, while $Br(h_1 \to gg)$ and $\Gamma^{tot}(h_1)$ we obtain using NMSSMtools.

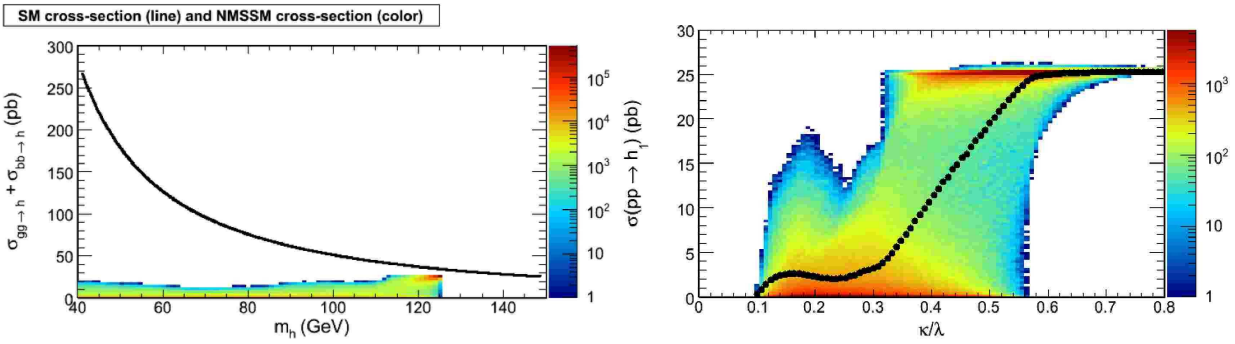

FIG. 11: Combined $\sigma(gg \to \mathcal{H}) + \sigma(b\bar{b} \to \mathcal{H})$ production cross section versus $m_{\mathcal{H}}$ for NMSSM and SM, where $\mathcal{H}$ stands either for NMSSM or SM Higgs boson.

The cross section of $b\bar{b} \to h_1$ was also evaluated at NLO as follows. The numerical calculation for the SM Higgs production in $b\bar{b} \to H_{SM}$ fusion has been carried out with the program developed in [33] and lately used also in [34] where the QCD-improved (running) Yukawa couplings have been used. Then using $Y_{bbh_1}/Y_{bbH_{SM}}$ ratio of Yukawa couplings calculated in NMSSMtools, one finds:

$$\sigma(b\bar{b} \to h_1) = \sigma(b\bar{b} \to H_{SM}) \left(\frac{Y_{bbh_1}}{Y_{bbH_{SM}}} \right)^2 \quad (4)$$

For the evaluation of production cross sections, CTEQ6M set for parton density function set was used.

Our first results on the combined $\sigma(gg \to \mathcal{H}) + \sigma(b\bar{b} \to \mathcal{H})$ production cross section versus $m_{\mathcal{H}}$ for NMSSM and SM are presented in Fig.11 (left), where $\mathcal{H}$ stands either for NMSSM or SM Higgs boson. The right frame of Fig.11 presents $\sigma(gg \to \mathcal{H}) + \sigma(b\bar{b} \to \mathcal{H})$ versus κ/λ for NMSSM in more details. (**Can we present(or think about how to present) also results for** $\sigma(gg \to \mathcal{H})$ $\sigma(b\bar{b} \to \mathcal{H})$ **separately to show their relative contribution?**). From Fig. 11 we can see that production cross section of NMSSM h_1 is indeed suppressed typically by 2 orders of magnitude as compared to the SM Higgs boson production in case

when h_1 has a significant singlet component. The value of the minimal suppression depends on the mass of h_1: for $m_{h1} \simeq 40 - 50$ GeV, the maximal cross section of h_1 production is about 10 smaller than the SM one, while when $m_{h1} \simeq 115 - 125$ GeV its production cross section is quite close to SM and can be as large as about 25 pb once the singlet component of h_1 vanishes.

Since we study the whole production and decay chain $pp \to h_1 \to a_1 a_1 \to 4\mu$ let us look at the cross section of the four-muon production after application of the respective branching ratios from NMMStoos to the h_1 production cross section which we have evaluated.

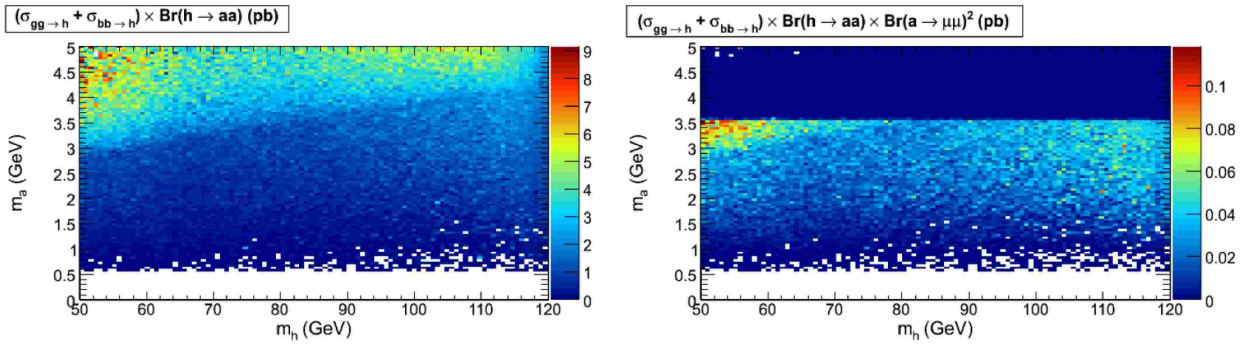

FIG. 12: $m_{a1} - m_{h1}$ plane with color map distribution of for $\sigma(gg + b\bar{b} \to h_1) \times Br(h_1 \to a_1 a_1)$ (left) and $\sigma(gg + b\bar{b} \to h_1) \times Br(h_1 \to a_1 a_1) \times Br(a_1 \to \mu\mu)^2$ (right) rates.

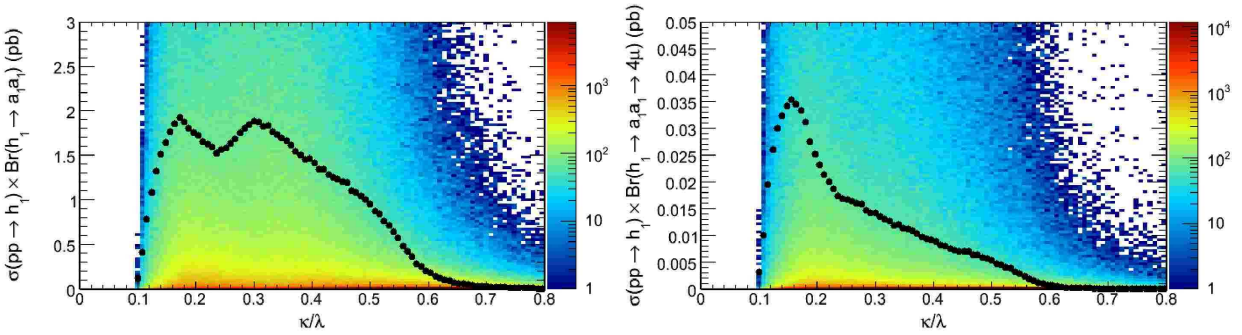

FIG. 13: Distribution of $\sigma(gg + b\bar{b} \to h_1) \times Br(h_1 \to a_1 a_1)$ (left) and $\sigma(gg + b\bar{b} \to h_1) \times Br(h_1 \to a_1 a_1) \times Br(a_1 \to \mu\mu)^2$ (right) (right) rates versus κ/λ.

In Fig.12 we present $m_{a1} - m_{h1}$ plane with color map distribution of for $\sigma(gg + b\bar{b} \to h_1) \times Br(h_1 \to a_1 a_1)$ (left) and $\sigma(gg + b\bar{b} \to h_1) \times Br(h_1 \to a_1 a_1) \times Br(a_1 \to \mu\mu)^2$ (right) rates. One can see that $\sigma(gg + b\bar{b} \to h_1) \times Br(h_1 \to a_1 a_1)$ rate can be quite large and reach about 10 pb for the light m_{h1} with the mass about 50 GeV. In the same time, the final cross section of the process

under study — $\sigma(gg+b\bar{b}\to h_1)\times Br(h_1\to a_1a_1)\times Br(a_1\to\mu\mu)^2 \equiv \sigma(gg+b\bar{b}\to h_1\to a_1a_1\to 4\mu)$ — can be only as large as about 0.1 pb. In Fig.13 we present details on the distribution of $\sigma(gg+b\bar{b}\to h_1)\times Br(h_1\to a_1a_1)$ (left) and $\sigma(gg+b\bar{b}\to h_1)\times Br(h_1\to a_1a_1)\times Br(a_1\to\mu\mu)^2$ (right) (right) rates versus κ/λ.

Even though the four-muon signal rates from NMSSM are not high, due to relatively low expected backgrounds the signature of our interest would allow us to exclude significant portion of NMSSM parameter space even at low integrated luminosities as we present below.

The parameter space accessible at the LHC at low and later on at high luminosity regime is quite unique since it can not be excluded by present low-energy experiments on rare B-meson decays since, as we have found the singlet component of the lightest CP-odd Higgs boson, a_1, is extremely close to unity. (**Please add here reference to the paper and the talks!**).

(**We should note that of course Tevatron is quite competitve with LHC on the search of 4μ signature from NMSSM since the production corss section at Tevatron is quite large. This is related to the fact that we study the system with comparatively small invariant mass which is not suppressed by gluon parton density since x-values are not large. On the other hand we should present a full potential of the LHC on covering the parameter space of 4μ signature from NMSSM down to high luminosity and compare Tevatron and LHC potentials in the Figure below.**) (**Another point we should probably**

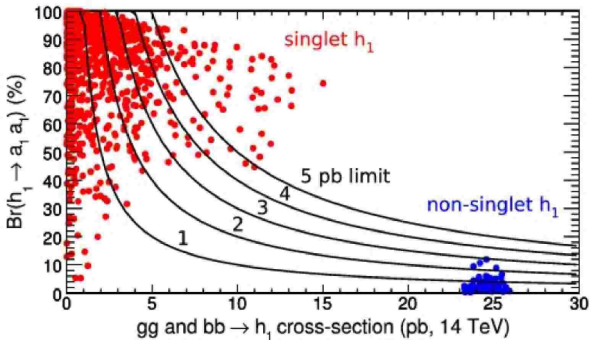

FIG. 14:

explore is to add $h2\to h_1h_1\to a_1a_1+X$ signature. Let me know if you need input from me on this subject. We have all ingredients for the production rate, so we

can easily add this cahnnel. We can add it in this section or later on.)

III. ANALYSIS

The main characteristic of the signal is two back-to-back di-muon pairs with pair consisting of spatially close muons. The di-muon pairs should have invariant masses consistent with each, which serve as a measurement of m_a, and the four muon invariant mass distributionshould have a spike that corresponding to the m_h mass. We use these striking features of signal events in designing the analysis with a reasonably high acceptance and very low backgrounds suitable for early LHC running.

A. Signal Simulation

We use Pythia to generate signal event templates with m_h in the range from 70 to 140 GeV/c^2 and m_a in the range from 0.5 to 4 GeV/c^2). For detector response emulation, we chose the CMS detector as a benchmark and used its parameters descibed in CMS Technical Design Report. The key parameters important for this analysis are muon momentum resolution, low threshold on muons to reach the muon system, acceptance and average muon reconstruction efficiencies. **we should quote the numbers.**

B. Event Reconstruction

The analysis starts by requiring at least four muon candidates with $p_T > 5$ GeV/$c$in the fiducial volume of the detector. At least one of the four muons has to have $p_T > 20$ GeV/c to suppress major backgrounds and to satisfy trigger requirements. Each event must have at least two muon candidates of positive and negative charge each. In events satisfying these critiria, we define quadruplets of candidates consisting of two positive and two negatively charged muon candidates. Although very unlikely, there can be more than one quadruplet per event, e.g. if there are five muons in the event. Each such quadruplet if preserved until the end of the analysis.

Next, we sort the four muon candidates in quadruplet into two di-muon pairs. We minimize the quantity $(\Delta R(\mu_i, \mu_j)^2 + \Delta R(\mu_k, \mu_l)^2)$ under the constarint that each di-muon

pair consists of two muon candidates of opposite charge. We discard quadruplets in which ΔR between muons in any of the two pair exceeds **0.5???** as this cut is 100% efficient for the signal while it can diminish the size of the data sample by removing events, which have topology inconsistent with signal. At his point in the analysis, the invariant mass of each of the di-muon pair, $m_{12} and m_{34}$, is calculated as well as the invariant mass of all four muons, which we denote as m_{1234} or M. Figure 15a) shows the invariant mass of the muon pairs passing all selections (m_{12} and m_{34} are combined into a single distribution) for two choices of m_h and m_a. Figure 15b) shows the distribution of the invariant mass M of the four muon system for two benchmark points. Further background suppression can be obtained by adding the isolation requirement to one or both di-muon pairs in the event, e.g. by setting the upper bound on the sum of transverse momenta of all tracks in a cone around the reconstructed direction of the di-muon pair excluding momenta of the two muon tracks. Such requirement can allow a very substantial suppression of the dominant source of the background coming from events with one or more muons originating from jets. We choose not to use this critirea as our estimates show that the final rate of such background events is already very low. If data shows larger contribution of these events, this isolation requirement would allow bringing backgrounds back to very low level at a moderate cost to signal acceptance.

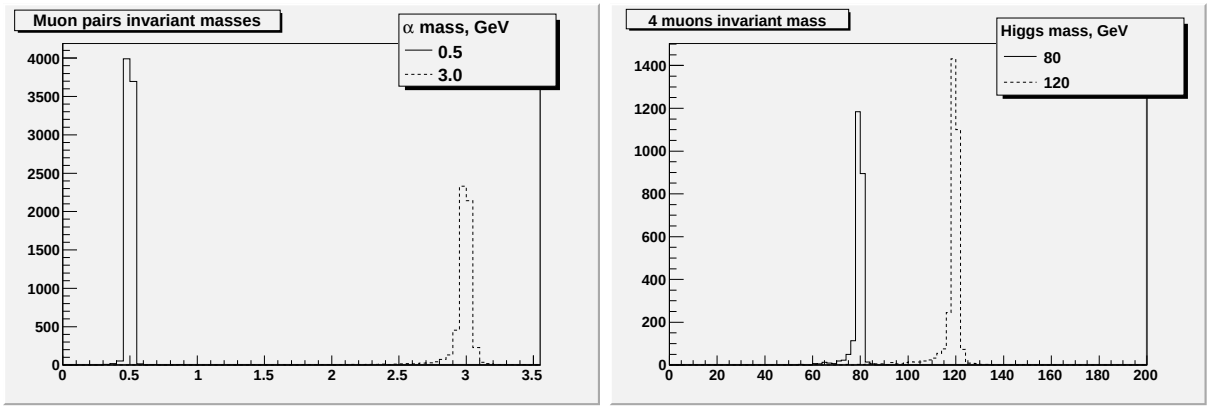

FIG. 15: Left: Reconstructed invariant mass of reconstructed muon pairs for $m_a = 0.5$ and 3 GeV/c^2 (in both cases $m_H = 100$ GeV/c^2). Right: Reconstructed invariant of four muons for $m_H = 80$ and $m_H = 120$ GeV/c^2 (in both cases $m_a = 3.0$ GeV).

Acceptance of the selections listed above is shown in Table II and is large thanks to the

TABLE II: Acceptances for various points in m_h-m_a space.

m_h, m_a (GeV)	0.5	1.0	2.0	3.0	4.0
80	0.3052 ± 0.0046	0.2656 ± 0.0044	0.2420 ± 0.0043	0.2389 ± 0.0043	0.2324 ± 0.0043
100	0.3915 ± 0.0049	0.3245 ± 0.0047	0.2906 ± 0.0045	0.2862 ± 0.0045	0.2819 ± 0.0045
120	0.4587 ± 0.0050	0.3785 ± 0.0049	0.3405 ± 0.0047	0.3226 ± 0.0047	0.3103 ± 0.0046

high coverage of the CMS muon system. Figures 16a) and 16b) illustrate the dependence of acceptance on values of m_h and m_a.

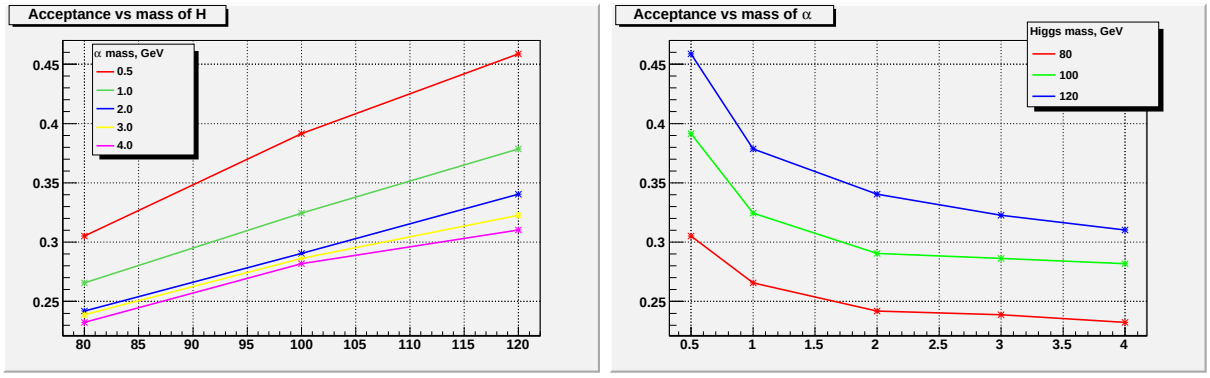

FIG. 16: Acceptance as a function of m_a for fixed m_h. Acceptance as a function of m_h for fixed m_a.

One can further reduce the background events and zoom on the region of interest of this analysis by applying cuts on m_{12}, m_{34}, M, and require that measured values of m_{12} and m_{34} are consistent within uncertainties. Instead of applying these cuts explicitly, we develop a statistical procedure that performs a fit in a 3D space of measured values of $(m_{12}, m_{34}, m_{1234})$ taking into account kinematical properties of signal events. This approach allows maximizing signal acceptance and therefore statistical power of the analysis and is discussed in what follows. It is also convenient from experimental point of view as the backgrounds will be distributed in some smooth fashion over the 3D space allowing fitting the 3D distribution to estimate backgrounds directly from the data. Potential signal would appear as a concentration of events in one specific region in the 3D space (a 3D "bump").

Figure 17 shows the difference in the reconstructed masses of the two di-muon pairs in signal events, which determines the size of the signal region in the (m_{12}, m_{34}) plane.

To give the reader a better idea on the signal significance of this analysis, we quote efficiencies and background contamination (next section) for a set of cuts that zooms on the highest significance region. The cuts we use are $M > 60$ GeV/c^2, $m_{12} < 4$, $m_{34} < 4$, and $|m_{12} - m_{34}| < 0.08 + 0.005 * (m_{12} + m_{34})$. The latter cut is enforcing the requirement that the two pair masses are consistent with each other and takes into account widening of the absolute resolution in the reconstructed di-muon mass as a function of mass.

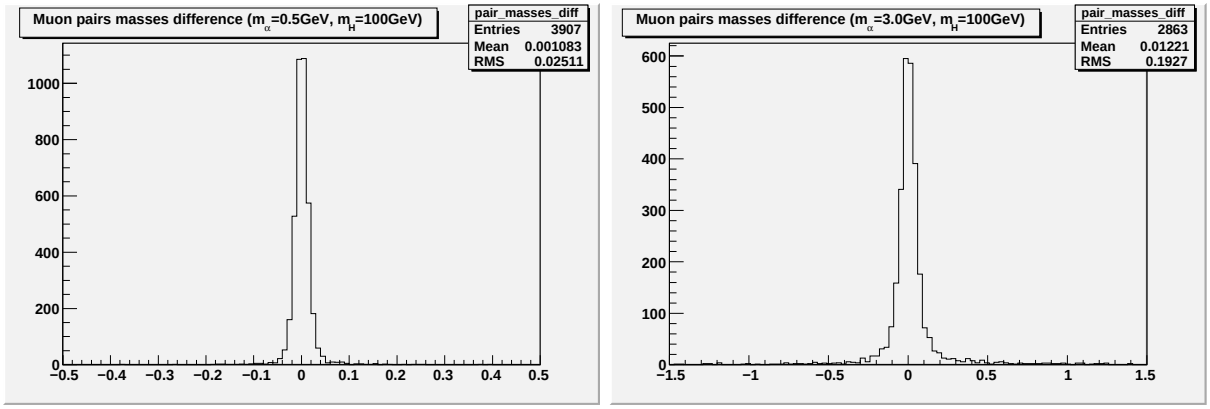

FIG. 17: Left: Muon pairs masses difference (m_a=0.5GeV, m_H=100 GeV). Right: Muon pairs masses difference (m_a=3.0GeV, m_H=100 GeV)

C. Background Estimation

The main backgrounds in this analysis are QCD multijet events where muons originate from either heavy flavor quark decays or from K/π decays in flight. We also considered electroweak backgrounds and direct J/psi production, but found those contributions completely negligible. Requirement of four sufficiently energetic muons in the event drastically reduces contributions of all background processes. Further constarints on the correlation of di-muon pair masses and relatively high invariant mass of the four muon system allows an essentially zero background analysis. In the following we discuss estimation of these backgrounds.

1. QCD backgrounds

The largest contribution comes from rare QCD multi-jet events with four energetic reconstructed muons that are produced either in heavy flavor decays of b and c mesons (real muons) or in K/π decays in flight. The punch-through contamination is heavily suppresed due to massive shileding of the CMS muon system. The multi-jet background is drastically reduced by the requirement of at least one muon with $p_T > 20$ GeV/c and the follow up selections. Background events surviving selections can be divided into two fractions: events with all four real muons from heavy flavor meson decays and events with typically three real muons and a misidentified muon from K/π decays in flight. The first source is estimated using Pythia MC 2→2 QCD jet production by selecting generated muons and smearing distributions using detector resolutions and efficiencies. The second contamination is estimated using the same Pythia sample by selecting events with two or three real muons and one or more charged pions or kaons satisfying p_T and η requirements used for muons. Each such event is assigned a weight calculated as the probability that available K/π mesons decay into muons before reaching radius of ≃2 meters (**halfway into the hadronic calorimeter - is it what we want?**). We find that the level of backgrounds due to misidentifications is comparable to the rate of the backgrounds associated with real muons from heavy flavor decays. While the fraction of remaining events after acceptance cuts does not appear negligible, these events are spread over the 3D space with only a tiny fraction of them appearing in the region where signal would appear, see Tables IV and VI. If necessary, these remaining backgrounds can be completely eliminated by applying a loose track isolation requirement on one of both of the di-muon pairs.

2. Electroweak four lepton backgrounds

We use CompHEP to generate a large sample of events with four muons in final state coming from the electroweak processes. The cross-section of this process is 0.5 pb (Sasha, is this correct? Kind of sounds very small!!!) and after a cut on the first muon $p_T > 20$ GeV/c, the large chunk of remaining events are $Z\gamma^*$ type events. Very few of these events have muons that can be arranged into pairs with low invariant mass, and the fraction of events with similar masses of

the pairs is completely negligible.

3. Other SM Backgrounds

We also studied several other processes, e.g. direct J/ψ production process that can produce a pair of muons with mass in the range of interest of this analysis and another pair of muons can come from decays in flight. We used Pythia MC and a weighing technique similar to the QCD case and find that this background is completely negligible. Other SM backgrounds (top, W+jets) are negligible in the region of interest of this analysis.

4. Summary

While the number of background events past the acceptance stage and that are used in the fit is not small, the fitting procedure described in the next section is effectively reducing the region of interest to events that have kinematic properties of signal events making backgrounds nearly completely negligible, as illustarted by the lower part of Table VI showing the number of expected background events after each cut in a dataset corresponding to 100 pb^{-1}of LHC data. **We need a plot to show background distributions, e.g. m12 and m1234 - we have them, just need to clean up**.

IV. STATISTICAL ANALYSIS OF THE DATA

To maximize sensitivity and emulate real data analysis techniques, we define a likelihood function in the 3D space ($m_{pair\,1}$, $m_{pair\,2}, M$), where M is the four muon invariant mass. The likelihood is defined as follows:

$$\mathcal{L}(m_h, m_a, \sigma(pp{\rightarrow}h)) = \prod_i \mathcal{P}(\sigma(pp{\rightarrow}h)\ L\ BR_{h\rightarrow aa} BR^2_{a\rightarrow\mu\mu} L\alpha(m_h, m_a) N_i^S(m_a, m_h) + L\ N_i^B, N_i^D) \quad (5)$$

where i runs over bins in 3D space of $(m_{12}, m_{34}, m_{1234})$, m_h is the light higgs mass, m_a is axial higgs mass, $\mathcal{P}(\nu, N)$ is Poisson probability for observing N events when the true rate is ν. Other parameters are dataset luminosity L, acceptance of the signal events $\alpha(m_h, m_a)$, N_i^S is the fraction of reconstructed signal events in bin i ($\Sigma N_i^S = 1$), N_i^B is the rate of background events in bin i per unit of luminosity.

TABLE III: Background cuts efficiency for generator level

Cuts	4 leptons	$\mu + x$	J/Ψ
1st eta<2.4	0.7994 ± 0.0040	0.95638 ± 0.00073	0.0088 ± 0.0022
2nd eta<2.4	0.8295 ± 0.0042	0.99992 ± 0.00003	$1.00^{+0.00}_{-0.06}$
3rd eta<2.4	0.8541 ± 0.0044	0.99584 ± 0.00024	0.75 ± 0.11
4th eta<2.4	0.7066 ± 0.0061	0.96407 ± 0.00068	0.75 ± 0.13
1st pt>5	0.9805 ± 0.0022	$1.00000^{+0}_{-0.00001}$	$1.0^{+0.0}_{-0.1}$
2nd pt>5	0.9405 ± 0.0038	0.8676 ± 0.0013	$1.0^{+0.0}_{-0.1}$
3rd pt>5	0.7893 ± 0.0068	0.0445 ± 0.0008	0.3333 ± 0.1571
4th pt>5	0.4390 ± 0.0093	0.0284 ± 0.0032	$0.00^{+0.27}_{-0.00}$
1st pt>20	0.9524 ± 0.0060	0.9873 ± 0.0126	0
analysis acceptance	0.1218 ± 0.0033	0.00099 ± 0.00011	0
pair masses<4	0.0025 ± 0.0014	0.3333 ± 0.0533	0
inv. mass>60	0.6667 ± 0.3333	0.4231 ± 0.0969	0
$\lvert m_{12} - m_{34} \rvert < 0.08$ $+0.005 * (m_{12} + m_{34})$	$X.XXXX \pm X.XXXX$	$X.XXXX \pm X.XXXX$	0
full efficiency	0.000203 ± 0.000143	0.00014 ± 0.00004	0

Because of the limited statistics in the Monte Carlo samples describing QCD backgrounds, we parameterize the background distriution in the (m_{12}, m_{34}, M) space using the following function:

$$B(m_{12}, m_{34}, m_{1234}) = f(m_{12}) \times f(m_{34}) \times g(m_{1234}) \tag{6}$$

$$f(m_{12}) = \tag{7}$$

$$g(m_{1234}) =, \tag{8}$$

This simple function describes backgrounds very well in the region of interest because typical four muon invariant mass values are much larger than the narrow range of di-muon pair masses effectively leading to very little correlation of the two. An important note is that using this parameterization requires that in the data analysis the order of pairs has to be randomized (e.g. designating m_{12} to be the mass of the pair that contains highest p_T muon

TABLE IV: Background cuts efficiency for reco level

Cuts	4 leptons	$\mu + x$	J/Ψ
1st pt>5	0.7455 ± 0.0044	$1.00000^{+0}_{-0.00001}$	$1.0000^{+0}_{-0.0006}$
2nd pt>5	0.7012 ± 0.0053	$1.00000^{+0}_{-0.00001}$	$1.0000^{+0}_{-0.0006}$
3rd pt>5	0.6066 ± 0.0068	0.04349 ± 0.0007	0.3333 ± 0.0013
4th pt>5	0.3300 ± 0.0084	0.0402 ± 0.0034	$0.00^{+0.15}_{-0.00}$
1st pt>20	0.9573 ± 0.0063	$1.000^{+0}_{-0.007}$	0
analysis acceptance	0.1002 ± 0.0030	0.0017 ± 0.0002	0
pair masses<4	0.0041 ± 0.0020	0.3358 ± 0.0403	0
inv. mass>60	0.50 ± 0.25	0.4348 ± 0.0731	0
$\lvert m_{12} - m_{34}\rvert < 0.08$ GeV			
$+0.005 * (m_{12} + m_{34})$	$X.XXXX \pm X.XXXX$	$X.XXXX \pm X.XXXX$	0
full efficiency	0.00020 ± 0.00014	0.00025 ± 0.00006	0

will break factorization), and so we randomize them in the analysis. Fitted parameters of the function are shown in Table **??**. We verified that background events found in MC are well described by this function by running pseudoexperiments using paramaterized distribution and verifying that the p-value for the outcome similar to what is observed in MC is high.

Thus defined likelihood function can be used to calculate the 95% C.L. upper limit on the cross-section times branching ratio of the $h \to \mu\mu\mu\mu$ signal or determine the intergrated luminosity required to make a discovery at a certain level. These results can then be translated into the exclusion region in (m_a, m_h) parameter space or NMSSM parameter space. To demonstrate performance of this technique, Figures 18a) and b) show calculated likelihood functions for two pseudoexperiments, in one of which no signal was injected into the pseudodata and in the other a certain amount of signal was admixed in addition to background contributions. In both cases, likelihood function shows expected behavior.

We calculate the 95% C.L. upper limit on the product $\sigma(pp \to h) B_{h \to aa} B^2_{a \to \mu\mu}\, \alpha$, using Bayesian technique which is 0.0293 pb at $L = 100$ pb^{-1}, approximately 3 events. In vast majority of pseudoexperiments, this limit is independent of m_h and m_a because the effective signal region that dominates signal significance in the fitter is essentially background free and

TABLE V: Expected number of background events after each selection cut on generator level

Cuts	4 leptons	Incl. muon	JPsi
Initial number	48.21 ± 0.49	152878.11 ± 546.06	120.91 ± 2.84
1st eta<2.4	38.54 ± 0.43	146209.61 ± 534.01	1.0652 ± 0.2663
2nd eta<2.4	31.97 ± 0.40	146197.91 ± 533.99	1.0652 ± 0.2663
3rd eta<2.4	27.30 ± 0.37	145589.38 ± 532.88	0.7989 ± 0.2306
4th eta<2.4	19.29 ± 0.31	140358.34 ± 523.22	0.5992 ± 0.1997
1st pt>5	18.92 ± 0.30	140358.34 ± 523.22	0.5992 ± 0.1997
2nd pt>5	17.79 ± 0.30	121774.70 ± 487.35	0.5992 ± 0.1997
3rd pt>5	14.04 ± 0.26	5424.13 ± 102.86	0.1997 ± 0.1153
4th pt>5	6.17 ± 0.17	154.08 ± 17.34	$0^{+0.067}_{-0.000}$
1st pt>20	5.87 ± 0.17	152.13 ± 17.23	$--$
pair masses<4	0.0147 ± 0.0085	50.71 ± 9.95	$--$
inv. mass>60	0.0098 ± 0.0069	21.45 ± 6.47	$--$
$\lvert m_{12} - m_{34}\rvert < 0.08$ GeV			
$+0.005 * (m_{12} + m_{34})$	$0.000^{+0.005}_{-0.000}$	$0.00^{+1.95}_{-0.00}$ **??**	$--$

probability to observe any pseudodata event is very small. Since $B_{a\to\mu\mu}$ is nearly a function of m_a only, it can be factored out, and the corresponding upper limit on $\sigma(pp\to h)B_{h\to aa}\alpha$ is presented in Table VII. The upper limit on $\sigma(pp\to h)B_{h\to aa}$ is shown as a function of m_h and m_a in Table VIII by factoring out α as well. Keep in mind that $B_{h\to aa}$ is close to 100% in much of our preferred region of NMSSM parameter space.

V. RESULTS

TO BE WRITTEN

TABLE VI: Expected number of background events after each selection cut on reco level

Cuts	4 leptons	Incl. muon	JPsi
Initial number	48.21 ± 0.49	152878.11 ± 546.06	120.91 ± 2.84
1st pt>5	35.94 ± 0.42	152878.11 ± 546.06	120.91 ± 2.84
2nd pt>5	21.20 ± 0.35	152878.11 ± 546.06	0.3995 ± 0.1631
3rd pt>5	15.29 ± 0.27	6648.99 ± 113.88	$0^{+0.067}_{-0.000}$
4th pt>5	5.04 ± 0.16	267.21 ± 22.83	$--$
1st pt>20	4.83 ± 0.15	267.21 ± 22.83	$--$
pair masses<4	0.0049 ± 0.0098	89.72 ± 13.23	$--$
inv. mass>60	0.0098 ± 0.0069	39.01 ± 8.72	$--$
$\lvert m_{12} - m_{34}\rvert < 0.08$ GeV			
$+0.005 * (m_{12} + m_{34})$	$0.000^{+0.005}_{-0.000}$	$0.00^{+1.95}_{-0.00}$ **??**	$--$

TABLE VII: 95% C.L. on $\sigma(pp{\to}h)B_{h\to aa}\,\alpha$ at $L = 100$ pb^{-1} as a function of m_a, from Fig **??**.

m_a (GeV)	$B_{a\to\mu\mu}$ (%)	$\sigma(pp{\to}h)B_{h\to aa}\,\alpha$ (pb)
0.5	0	∞
0.75	4.2	16.5
1.0	10.0	2.9
1.5	15.7	1.2
2.0	17.2	1.0
2.5	17.1	1.0
3.0	16.1	1.1
3.5	14.8	1.3
3.75	1.02	282
4.0	0.73	557
5.0	0.49	1220

TABLE VIII: 95% C.L. on $\sigma(pp{\to}h)B_{h\to aa}$ (pb) at $L = 100$ pb^{-1}, from Fig **??** and Table II.

m_h, m_a (GeV)	0.5	1.0	2.0	3.0	4.0
80	∞	10.9	4.1	4.6	2400
100	∞	8.9	3.4	3.8	2000
120	∞	7.7	2.9	3.4	1800

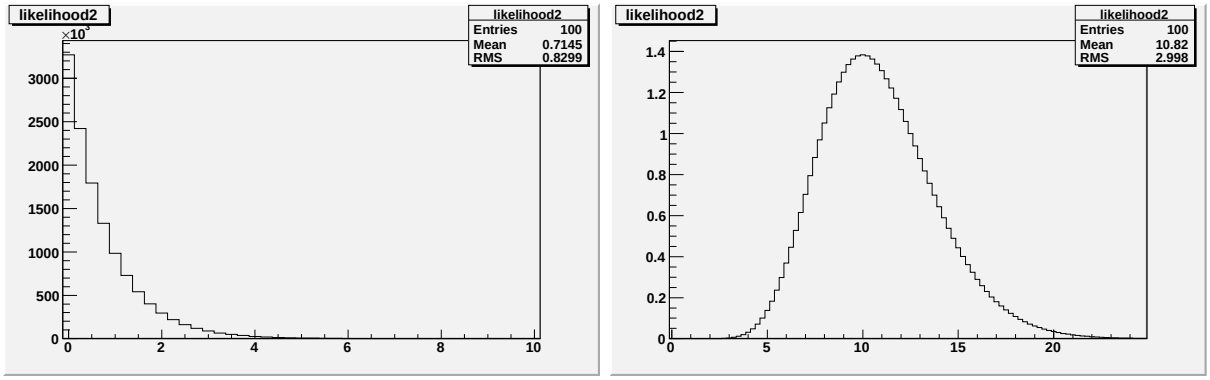

FIG. 18: Left:Example likelihood for a pseudoexperiment for a search assuming $B(H{\to}aa{\to}\mu\mu\mu\mu)$=0.04, $m_a = 3$ GeV, $m_h = 100$ GeV with null signal shows that a 95% exclusion is somewhere around 2.5 pb for $\sigma(pp{\to}H)$. Right: Example likelihood for $\sigma(pp{\to}H)$=10 pb^{-1}, $B(H{\to}aa{\to}\mu\mu\mu\mu)$=0.04, $m_a = 3$ GeV $m_h = 100$ GeV shows a more than 5σ observation.

Acknowledgments

We thank XXX and YYY

[1] H. P. Nilles, M. Srednicki and D. Wyler, Phys. Lett. B **120** (1983) 346.
[2] J. M. Frere, D. R. T. Jones and S. Raby, Nucl. Phys. B **222** (1983) 11.
[3] J. R. Ellis, J. F. Gunion, H. E. Haber, L. Roszkowski and F. Zwirner, Phys. Rev. D **39** (1989) 844.
[4] M. Drees, Int. J. Mod. Phys. A **4** (1989) 3635.
[5] U. Ellwanger, Phys. Lett. B **303** (1993) 271 [arXiv:hep-ph/9302224].
[6] U. Ellwanger, M. Rausch de Traubenberg and C. A. Savoy, Phys. Lett. B **315** (1993) 331 [arXiv:hep-ph/9307322].

[7] T. Elliott, S. F. King and P. L. White, Phys. Rev. D **49** 2435 (1994) 2435 [arXiv:hep-ph/9308309].

[8] P. N. Pandita, Z. Phys. C **59** (1993) 575.

[9] U. Ellwanger, M. Rausch de Traubenberg and C. A. Savoy, Z. Phys. C **67** (1995) 665 [arXiv:hep-ph/9502206].

[10] S. F. King and P. L. White, Phys. Rev. D **52** (1995) 4183 [arXiv:hep-ph/9505326].

[11] F. Franke and H. Fraas, Int. J. Mod. Phys. A **12** (1997) 479 [arXiv:hep-ph/9512366].

[12] U. Ellwanger, M. Rausch de Traubenberg and C. A. Savoy, Nucl. Phys. B **492** (1997) 21 [arXiv:hep-ph/9611251].

[13] D. J. Miller, R. Nevzorov and P. M. Zerwas, Nucl. Phys. B **681** (2004) 3.

[14] J. E. Kim and H. P. Nilles, Phys. Lett. B **138**, 150 (1984).

[15] R. Dermisek and J. F. Gunion, Phys. Rev. Lett. **95**, 041801 (2005) [arXiv:hep-ph/0502105].

[16] B. A. Dobrescu, G. L. Landsberg and K. T. Matchev, Phys. Rev. D **63**, 075003 (2001) [arXiv:hep-ph/0005308]; B. A. Dobrescu and K. T. Matchev, JHEP **0009**, 031 (2000) [arXiv:hep-ph/0008192].

[17] J. F. Gunion, H. E. Haber and T. Moroi, *In the Proceedings of 1996 DPF / DPB Summer Study on New Directions for High-Energy Physics (Snowmass 96), Snowmass, Colorado, 25 Jun - 12 Jul 1996, pp LTH095* [arXiv:hep-ph/9610337]; U. Ellwanger, J. F. Gunion and C. Hugonie, arXiv:hep-ph/0111179

[18] J. R. Ellis, J. F. Gunion, H. E. Haber, L. Roszkowski and F. Zwirner, Phys. Rev. D **39**, 844 (1989); B. A. Dobrescu, G. L. Landsberg and K. T. Matchev, Phys. Rev. D **63**, 075003 (2001) [arXiv:hep-ph/0005308];
U. Ellwanger, J. F. Gunion, C. Hugonie and S. Moretti, arXiv:hep-ph/0305109; U. Ellwanger, J. F. Gunion, C. Hugonie and S. Moretti, arXiv:hep-ph/0401228; U. Ellwanger, J. F. Gunion and C. Hugonie, JHEP **0507**, 041 (2005) [arXiv:hep-ph/0503203].

[19] S. Moretti, S. Munir and P. Poulose, Phys. Lett. B **644**, 241 (2007) [arXiv:hep-ph/0608233];

[20] S. Chang, P. J. Fox and N. Weiner, Phys. Rev. Lett. **98**, 111802 (2007) [arXiv:hep-ph/0608310].

[21] R. Dermisek and J. F. Gunion, Phys. Rev. D **75**, 075019 (2007) [arXiv:hep-ph/0611142].

[22] K. Cheung, J. Song and Q. S. Yan, Phys. Rev. Lett. **99**, 031801 (2007) [arXiv:hep-ph/0703149].

[23] J. R. Forshaw, J. F. Gunion, L. Hodgkinson, A. Papaefstathiou and A. D. Pilkington, JHEP **0804** (2008) 090 [arXiv:0712.3510 [hep-ph]].

[24] A. Belyaev, S. Hesselbach, S. Lehti, S. Moretti, A. Nikitenko and C. H. Shepherd-Themistocleous, arXiv:0805.3505 [hep-ph].

[25] A. Menon, D. E. Morrissey and C. E. M. Wagner, Phys. Rev. D **70** (2004) 035005 [arXiv:hep-ph/0404184]; D. G. Cerdeno, C. Hugonie, D. E. Lopez-Fogliani, C. Munoz and A. M. Teixeira, JHEP **0412** (2004) 048 [arXiv:hep-ph/0408102]; G. Belanger, F. Boudjema, C. Hugonie, A. Pukhov and A. Semenov, JCAP **0509**, 001 (2005) [arXiv:hep-ph/0505142]; J. F. Gunion, D. Hooper and B. McElrath, Phys. Rev. D **73**, 015011 (2006) [arXiv:hep-ph/0509024]; F. Ferrer, L. M. Krauss and S. Profumo, Phys. Rev. D **74**, 115007 (2006) [arXiv:hep-ph/0609257]; D. G. Cerdeno, E. Gabrielli, D. E. Lopez-Fogliani, C. Munoz and A. M. Teixeira, JCAP **0706**, 008 (2007) [arXiv:hep-ph/0701271]; C. Hugonie, G. Belanger and A. Pukhov, JCAP **0711**, 009 (2007) [arXiv:0707.0628 [hep-ph]]; V. Barger, P. Langacker, I. Lewis, M. McCaskey, G. Shaughnessy and B. Yencho, Phys. Rev. D **75**, 115002 (2007) [arXiv:hep-ph/0702036]. S. Kraml, A. R. Raklev and M. J. White, Phys. Lett. B **672**, 361 (2009) [arXiv:0811.0011 [hep-ph]]; G. Belanger, C. Hugonie and A. Pukhov, JCAP **0901**, 023 (2009) [arXiv:0811.3224 [hep-ph]].

TABLE IX: Background samples normalization

Sample	σ	N_{evt}^{gen}	Filter efficiency	L_{eff}	$f = L_{100}/L_{eff}$
$\mu + x$	$0.5091mb$	6238383	0.000239	$51.2709pb^{-1}$	1.9504
4 leptons	$0.538pb$	10995	1.0	$20436.803pb^{-1}$	0.0049
J/ψ	$0.127.2nb$	1413803	0.0074	$1502.00pb^{-1}$	0.0666

[26] U. Ellwanger, J.F. Gunion and C. Hugoine, JHEP **0502**, 066 (2005).
[27] U. Ellwanger, C. Hugoine, Comput. Phys. Commun. **175**, 290 (2006).
[28] F. Domingo and U. Ellwanger, arXiv:0710.3714 [hep-ph].
[29] G. Abbiendi *et al.* (OPAL Collaboration), Eur. Phys. J. C **18**, 425-445 (2001).
[30] G. Abbiendi *et al.* (OPAL Collaboration), Eur. Phys. J. C **27**, 483-495 (2003), arXiv:0209068v1 [hep-ex].
[31] M. Spira, A. Djouadi, D. Graudenz and P. M. Zerwas, Nucl. Phys. B **453**, 17 (1995) [arXiv:hep-ph/9504378].
[32] A. Djouadi, J. Kalinowski and M. Spira, Comput. Phys. Commun. **108**, 56 (1998) [arXiv:hep-ph/9704448].
[33] C. Balazs, H. J. He and C. P. Yuan, Phys. Rev. D **60**, 114001 (1999) [arXiv:hep-ph/9812263].
[34] A. Belyaev, J. Pumplin, W. K. Tung and C. P. Yuan, JHEP **0601**, 069 (2006) [arXiv:hep-ph/0508222].

VI. APPENDIX